

## Supplementary information

### 1 Large experimental angle of repose values reported for the single bead ensembles

The values of the angle of repose (AoR) usually attributed to steel beads are calculated experimentally for nearly perfectly spherical particles. The beads used in this study are obtained by cutting the links in industrially manufactured chains and isolating the individual beads. These beads have many characteristics that separate them from spherical and monodisperse bead ensembles, such as:

- a) The shape of the individual beads is ellipsoidal and the presence of the cavity transforms the shape into hollow drum-like. This drum shaped particle has two sharp edges, thus flat faces on the two ends. These shape characteristics increase the eccentricity of the contact normal directions for these particles (Fig. S1).
- b) The major and minor axis of the particles is  $2.1 \pm 0.1$  mm and  $2.0 \pm 0.1$  mm long respectively, which provides a range of particle sizes and shapes (Fig. S1).

The non-sphericity [1-4] and presence of flat faces/edges [5] has been reported to increase the angle of repose of granular ensembles. The large experimental angle of repose reported for the single beads ( $30^\circ$ ) is therefore attributed to the shape characteristics of the beads [6]. In the case of chain ensembles of length  $M = 4, 12$  and  $24$ , the presence of links prevents the flat edges/faces of the beads from contact formation. Therefore, the effects of particle non-sphericity are absent in chain ensembles. Following the above reasoning, the coefficient of sliding friction and coefficient of rolling friction were calibrated separately for single bead ensembles ( $M = 1$ ) and for the chain ensembles ( $M = 4, 12, 24$ ).

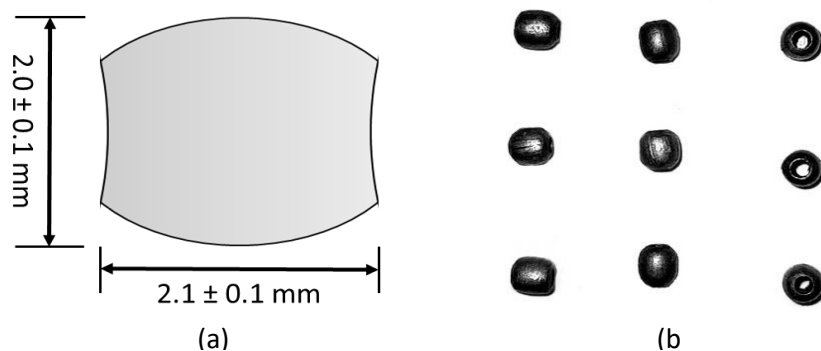


Fig S1: (a) Schematic showing the geometry of the beads. (b) Photo of beads showing the view of beads from three axes.

## 2 Friction coefficient values calibration

An indirect method for incorporating non-spherical particle shapes is using friction coefficients, in particular the rolling friction coefficient, as explored by Wensrich et al., 2012 [7] and Soltanbeigi et al., 2021 [5]. As finding a unique pair of friction coefficients for a given angle of repose is underdetermined [8,9] i.e. multiple pairs of sliding and rolling friction coefficient values ( $\mu_s$ ,  $\mu_r$ ) result in same angle of repose, therefore for simplicity, in our study we assume the angle of sliding friction and coefficient of rolling friction to be equal. Fig. S2 shows the angle of repose and corresponding friction coefficient values for single beads and chains of length  $M = 4$  (Chains of length  $M = 12$  and  $24$  do not form conical piles at non-zero friction coefficients). From our simulation sweeps the best fitting values of friction coefficients for single bead (AoR =  $30^\circ$ ) and chain ensembles (AoR =  $34^\circ$ ) were obtained to be 0.4 and 0.25 respectively. In order to incorporate the effect of non-spherical shapes of beads in single bead ensembles, the adopted values for friction coefficients are higher than that of perfectly spherical particles of same material, similar to as reported by Wensrich et al., 2012[7] and Li et al., 2013[9] etc.

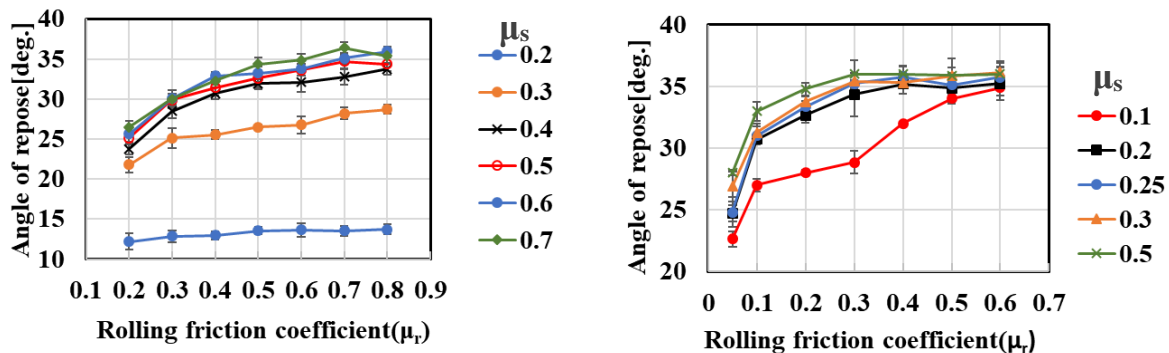


Fig S2: (a) Variation of angle of repose of ( $M = 1$ ) bead ensemble with sliding( $\mu_s$ ) and rolling( $\mu_r$ ) friction coefficient. (b) Variation of angle of repose of ( $M = 4$ ) chain ensemble with sliding( $\mu_s$ ) and rolling( $\mu_r$ ) friction coefficient.

### 3 List of simulations performed

The total simulation sweeps performed in the study are shown in the matrix given in Fig. S3. The number in each box is the initial state aspect ratio ( $AR_i$ ) of the ensemble. All the ensembles are compacted at their densest packing fraction. The initial state densest packing fraction is a function of the chain length( $M$ ) as reported by Sarate et al., 2022[6]. The number of particles is fixed at  $\sim 6000$  for each simulation. As the ensembles in smaller diameter cylinders don't form stable columns because of their high initial aspect ratio (Movie S1) and the larger diameter cylinder form columns of small height (i.e. Small  $A.R_i$ ), the intermediate case of cylinder diameter of 35 mm is adopted as the geometry for studying the force transmission in standing columns (Movie S2). The details of simulations for this case are provided in table S1.

















	<b>M = 1</b>	<b>M = 4</b>	<b>M = 12</b>	<b>M = 24</b>
<b>D = 16mm</b>	 15	 16.3	 22	 22.1
<b>D = 22mm</b>	 5	 5.1	 7.2	 7.2
<b>D = 35mm</b>	 1.5	 1.55	 2.3	 2.3
<b>D = 60mm</b>	 0.3	 0.3	 0.41	 0.41

Fig. S3: Simulation sweeps conducted in this study by varying the initial geometry of the cylindrical container.

Table S1: Simulation parameters for the case of ensembles in cylinder of diameter 35mm.

<b>Chain length, M</b>	<b>No. of particles</b>	<b>No. of chains</b>	<b>No. of simulation runs</b>	<b>Initial Aspect ratio</b>	<b>Initial packing fraction</b>
N = 1	6000	-	30	1.5	0.55
N = 4	6000	1500	25	1.55	0.50
N = 12	6000	500	25	2.3	0.43
N = 24	6000	250	25	2.3	0.43

## 4 Compaction of the chain ensembles

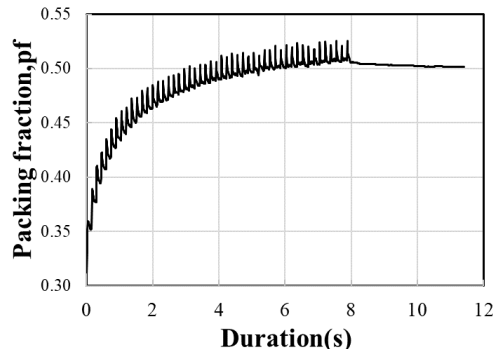


Fig. S4: The cumulative compaction of the chain ensemble ( $M = 4$ ) by vertical velocity impulses simulating laboratory tamping

The chain ensembles are generated by creating the chains one at a time and letting them fall into the cylinder under the gravity. After all the chains are deposited, all the beads in the ensemble are given downward velocity impulses of 1.4 m/s, equivalent to dropping the cylinder from a height of 10cm. Successive vertical impulses (tamping) are applied until the ensembles are compacted to their densest packing fraction (Fig. S4) as reported by Sarate et.al (2022)[6].

## 5 Calibration of the link contact model parameters

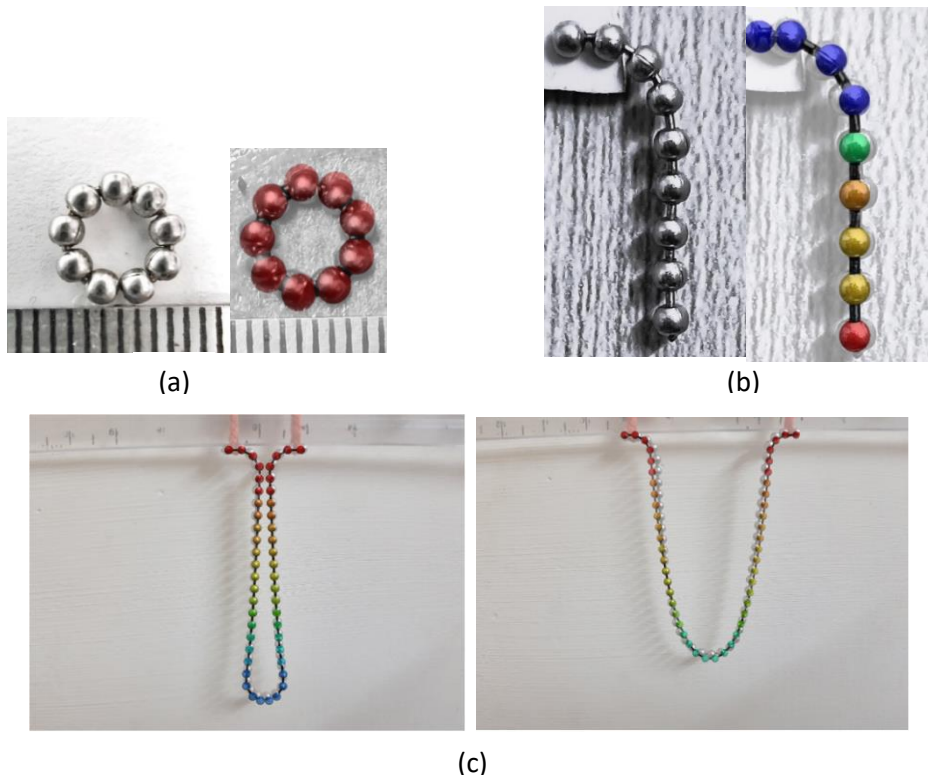


Fig. S5: (a) Comparison of the closed loop formed by the metallic chain and modelled chain. (b) Final configuration of a chain under gravity and its comparison with modelled chain. (c) Superimposed configurations of catenary shape formed by actual and modelled chain of length  $M = 48$  beads.

The implemented link contact model is calibrated against the characteristic deformation patterns of the individual chains. We calibrate the link contact model parameters  $k_{nt1}$ ,  $k_{nt2}$  and  $k_{\theta}$  by replicating the deformation patterns of actual metallic chains as closely as possible under similar boundary conditions. As the stiffness  $k_{nt1}$  represents a small nominal stiffness, it is assigned a value of 1 N/m, which practically allows the unrestricted elongation of the links up to  $l_0 = 1\text{mm}$ .

The values of  $k_{nt2}$  and  $k_{\theta}$  are obtained from comparing the deformation of modelled and metallic chains in following three cases:

- a) As the angle between two links cannot be smaller than 140 degrees, thus when curled, these chains form the smallest closed loop with a chain of length 9 beads. Similar curling pattern is also captured by the modelled chain of length  $M = 9$  when a radial velocity is applied on the end beads of the chain (Fig. S5 a) (Movie S5).
- b) We also compare the oscillations and final shape of the metallic chain under gravity, when fixed by its first link. The deformed configurations of the modelled chain show close agreement with that of the metallic chains (Fig. S5 b) (Movie S6).
- c) Similarly, we calibrate against the characteristic catenary shape formed by a chain of length 48 beads when its ends are slowly moved towards each other at a velocity of 1cm/sec (Fig. S5 c) (Movie S7).

From comparing the superimposed deformed shapes of the modelled and actual chains, the best fitting value of  $k_{nt2}$  and  $k_{\theta}$  are obtained as  $1e4$  N/m and 50N/deg. respectively.

## 6 Movie captions

Movie S1. This movie shows the column buckling and subsequent conical pile formation by chain ensemble of high initial aspect ratio ( $A.R_i = 7.2$ ). Different chains are shown in different colour and link contacts are shown as black coloured cylinders connecting beads. The diameter of the cylinder is 22mm and the chain length  $M = 12$  beads. Total number of beads in the ensemble is  $\sim 6000$ .

Movie S2. This movie shows the stable column formation by chains of length  $M = 12$ . The diameter of the cylinder is 35mm with an initial aspect ratio ( $A.R_i$ ) of 2.3. Total number of beads in the ensemble is  $\sim 6000$ . Different chains are shown in different colour and link contacts are shown as black coloured cylinders connecting beads.

Movie S3. This movie shows the stable column formation by chains of length  $M = 24$ . The diameter of the cylinder is 35mm with an initial aspect ratio(A.Ri) of 2.3. Total number of beads in the ensemble is ~6000. Different chains are shown in different colour and link contacts are shown as black coloured cylinders connecting beads.

Movie S4. This movie shows the conical pile formation by chains of length  $M = 4$ . The diameter of the cylinder is 35mm with an initial aspect ratio(A.Ri) of 1.55. Total number of beads in the ensemble is ~6000. Different chains are shown in different colour and link contacts are shown as black coloured cylinders connecting beads.

Movie S5. This movie shows the closed link formation by a modelled chain of length  $M = 9$  beads. The deformation results from application of radial velocity on the end beads of the chain. The beads are shown in red colour and link contact shown as black cylinders connecting particles.

Movie S6. This movie shows the oscillations and final shape of a chain of length  $M = 9$ , falling under gravity when held fixed by the first link. The beads are coloured by their velocity and the link contacts are shown as black coloured cylinders connecting beads.

Movie S7. This movie shows the characteristic catenary shape formation by a chain of length  $M = 48$ , when its ends are brought closer to each other. The beads are coloured by their velocity and the link contacts are shown as black coloured cylinders connecting beads.

## References

- 1) Zhou, Z.Y., Zou, R.P., Pinson, D. and Yu, A.B., 2014. Angle of repose and stress distribution of sandpiles formed with ellipsoidal particles. *Granular Matter*, 16(5), pp.695-709.
- 2) Dai, B.B., Yang, J. and Zhou, C.Y., 2017. Micromechanical origin of angle of repose in granular materials. *Granular Matter*, 19(2), pp.1-10.
- 3) Chen, H., Zhao, S. and Zhou, X., 2020. DEM investigation of angle of repose for super-ellipsoidal particles. *Particuology*, 50, pp.53-66.
- 4) Gallas, J.A. and Sokolowski, S., 1993. Grain non-sphericity effects on the angle of repose of granular material. *International Journal of Modern Physics B*, 7(09n10), pp.2037-2046.
- 5) Soltanbeigi, B., Podlozhnyuk, A., Kloss, C., Pirker, S., Ooi, J.Y. and Papanicolopoulos, S.A., 2021. Influence of various DEM shape representation methods on packing and shearing of granular assemblies. *Granular Matter*, 23(2), pp.1-16.
- 6) Sarate, P.S., Murthy, T.G. and Sharma, P., 2022. Column to pile transition in quasi-static deposition of granular chains. *Soft Matter*, 18(10), pp.2054-2059.
- 7) Wensrich, C.M. and Katterfeld, A., 2012. Rolling friction as a technique for modelling particle shape in DEM. *Powder Technology*, 217, pp.409-417.
- 8) Zhou, Y.C., Xu, B.H., Yu, A.B. and Zulli, P., 2001. Numerical investigation of the angle of repose of monosized spheres. *Physical Review E*, 64(2), p.021301.
- 9) Li, Q., Feng, M. and Zou, Z., 2013. Validation and calibration approach for discrete element simulation of burden charging in pre-reduction shaft furnace of COREX process. *ISIJ international*, 53(8), pp.1365-1371.